Accepted Manuscript

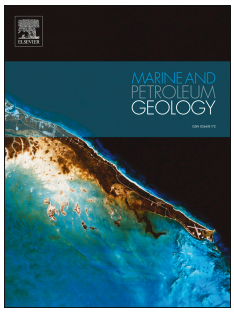

Modelling persistent methane seepage offshore western Svalbard since early Pleistocene

Jochen Knies, Matthias Daszinnies, Andreia Plaza-Faverola, Shyam Chand, Øyvind Sylta, Stefan Bünz, Joel E. Johnson, Rune Mattingsdal, Jürgen Mienert

PII: S0264-8172(18)30020-5

DOI: 10.1016/j.marpetgeo.2018.01.020

Reference: JMPG 3210

To appear in: *Marine and Petroleum Geology*

Received Date: 7 June 2017

Revised Date: 11 December 2017

Accepted Date: 16 January 2018

Please cite this article as: Knies, J., Daszinnies, M., Plaza-Faverola, A., Chand, S., Sylta, Ø., Bünz, S., Johnson, J.E., Mattingsdal, R., Mienert, Jü., Modelling persistent methane seepage offshore western Svalbard since early Pleistocene, *Marine and Petroleum Geology* (2018), doi: 10.1016/j.marpetgeo.2018.01.020.

This is a PDF file of an unedited manuscript that has been accepted for publication. As a service to our customers we are providing this early version of the manuscript. The manuscript will undergo copyediting, typesetting, and review of the resulting proof before it is published in its final form. Please note that during the production process errors may be discovered which could affect the content, and all legal disclaimers that apply to the journal pertain.

ACCEPTED MANUSCRIPT

Modelling persistent methane seepage offshore western Svalbard since Early Pleistocene

Jochen Knies[1,2], Matthias Daszinnies[3], Andreia Plaza-Faverola[2], Shyam Chand[1,2], Øyvind Sylta[3], Stefan Bünz[2], Joel E. Johnson[2,4], Rune Mattingsdal[5], Jürgen Mienert[2]

[1]*Geological Survey of Norway, NO-7491 Trondheim, Norway*

[2]*CAGE - Centre for Arctic Gas Hydrate, Environment and Climate; Department of Geosciences, UiT The Arctic University of Norway, NO-9037 Tromsø, Norway*

[3]*Migris AS, NO-7462 Trondheim, Norway*

[4]*Department of Earth Sciences, University of New Hampshire, 56 College Road, Durham, New Hampshire 03824, USA*

[5]*Norwegian Petroleum Directorate, NO-9488 Harstad, Norway*

ACCEPTED MANUSCRIPT

Abstract

Recent observations of extensive methane release into the oceans and atmosphere have raised concern as to whether rising temperatures across the Arctic could drive rapid destabilization of gas hydrate reservoirs. Here, we report modelling results from hydrate-modulated methane seepage from Vestnesa Ridge, offshore western Svalbard, suggesting that continuous leakage has occurred from the seafloor since the early Pleistocene up until today. Sustained by modelled deep subsurface thermogenic sources of Miocene age, large scale hydrocarbon fluid migration started ~6 million years ago and reached the seafloor some 4 million years later. The modelling results indicate that widespread methane seepage offshore western Svalbard commenced in earnest during early Pleistocene, significantly older than late Holocene as previously reported. We propose that the onset of vertical hydrocarbon migration is the response of rapid burial of potential hydrocarbon sources induced by increased sediment deposition following the onset of Northern Hemisphere glaciations, ~2.7 million years ago. From the modelling results we propose that source rock intervals capable of generating hydrocarbons and hydrocarbon reservoirs buried kilometers deep have continuously fueled the gas hydrate system off western Svalbard for the past 2 million years. It is this hydrocarbon system that primarily controls the thermogenic methane fluxes and seepage variability at the seabed over geological times.

ACCEPTED MANUSCRIPT

1. Introduction

Quantifying the release of methane and other potent greenhouse gases sequestered as submarine gas hydrates is critical for understanding the drivers of past and predicting future climate trajectories (Ruppel, 2011). Across the Arctic, recent discoveries of natural gas actively venting into the water column have been attributed to the thermal destabilization of shallow gas hydrate reservoirs due to ongoing thawing of offshore permafrost coupled with ocean bottom warming (Shakhova et al., 2014; Westbrook et al., 2009). It is estimated that current Arctic warming will release ~50 Gt of hydrate-sourced methane from the East Siberian Shelf into the atmosphere during our current decade up to 2025 (Whiteman et al., 2013), a flux that is apparently unprecedented during the Quaternary record (Loulergue et al., 2008). However, gas flares in the water column can also emerge from natural pathways that enable fluids to migrate from deep thermogenic hydrocarbon sources directly to the seabed over millions of years. Furthermore, recent geophysical evidence reveals that a prominent cluster of gas flares detected off the western Svalbard coast has existed for at least 3000 years (Berndt et al., 2014) implying that gas leakage into the ocean has continued throughout this time independent of climatic fluctuations (i.e.,the Little Ice Age and Medieval Optimum). To date, there are virtually no constraints on long-term variability in gas leakage rates across the Arctic or, specifically, on the origin of the leaking gas and the spatial and temporal evolution of hydrate-controlled methane seepage (Dumke et al., 2016; Plaza-Faverola et al., 2015; Plaza-Faverola et al., 2017).

ACCEPTED MANUSCRIPT

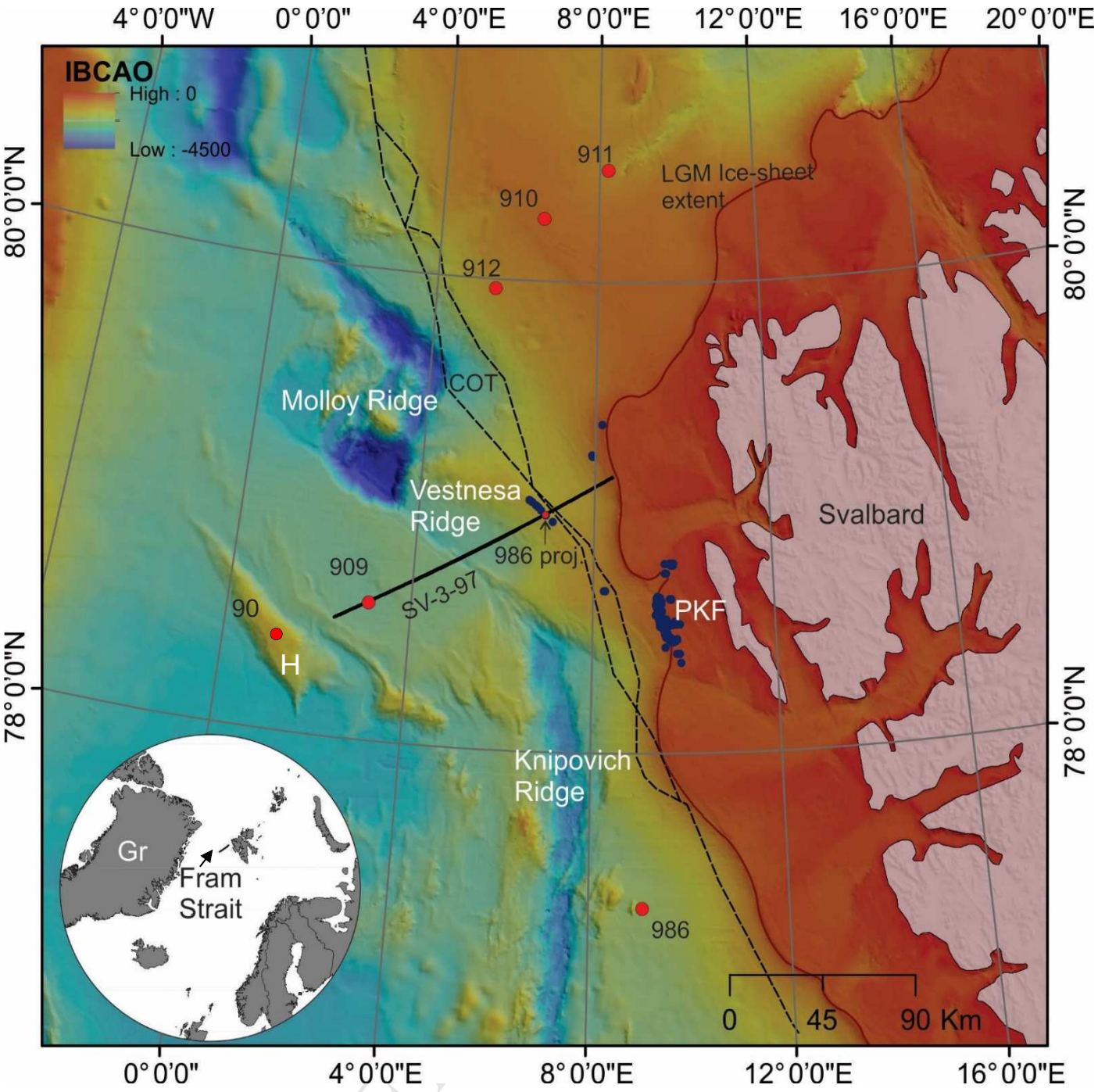

Fig. 1 The Arctic-Atlantic gateway (Fram Strait) in the Nordic Seas (inset), bathymetry (IBCAO, International Bathymetric Chart of the Arctic Ocean) (Jakobsson et al., 2012), and location of 2D seismic profile SV-3-97 and Ocean Drilling Program (ODP) Sites 910-912 (Yermak Plateau), 909-908 (Fram Strait), and 986 (western Svalbard). Detected gas flares on Vestnesa Ridge and Prins Karls Forland (PKF) are indicated by blue dots. The projection of Site 986 on seismic profile SV-3-97 is indicated. Continent-ocean boundary (COB) is modified from Engen et al. (2008) Gr: Greenland, HR: Hovgård Ridge.

ACCEPTED

In order to circumvent this problem and assess variability in long-term gas leakage we modelled a petroleum system that predicts methane generation and migration from thermogenic sources to the leakage points in the Atlantic-Arctic gateway region over millions of years. The model is constrained by one 2D seismic reflection profile (SV-3-97) tied to available borehole data (Fig. 1; Table 1). The seismic profile reveals a complete marine late Cenozoic sequence; at least ~17 million years of sedimentary section is inferred from Ocean Drilling Program (ODP) Site 909 biostratigraphic data compilation (Matthiessen et al., 2009; Myhre et al., 1995; Winkler et al., 2002; Wolf-Welling et al., 1996), that crosses a region with active methane seepage located along the western Svalbard margin (Figs. 1 and 2) (Bünz et al., 2012). In the west, the 2D seismic reflection profile SV-3-97 is tied to ODP Site 909, in which organic-rich (>2 wt.%) deposits of largely terrigenous origin and free gas anomalies have been detected (Stein et al., 1995). In the east, the same 2D profile crosses the gas hydrate reservoir and associated seepage system of the easternmost segment of the Vestnesa Ridge, which is defined as a contourite drift located north of the Molloy transform fault (Fig. 2) (Bünz et al., 2012; Fisher et al., 2011; Hustoft et al., 2009; Smith et al., 2014).

ACCEPTED MANUSCRIPT

SEE: SEPARATE FIGURE 2

ACCEPTED MANUSCRIPT

Fig. 2. 2D seismic profile SV-3-97 and depth-converted interpretations (in meters) with faults and age assignments (Ma, millions of years). (A): Seismic profile SV-3-97 (in TWT = two-way travel-time) with fault interpretation and position of ODP Site 909, Molloy Transform Fault (MTF), and Vestnesa Ridge gas flares (VR gas). Color codes: Red (1) = seafloor; Yellow (2) = 2.6 Ma (Matuyama-Gauss chron boundary) (Mattingsdal et al., 2014); Green (3) = 6.2 Ma (biostratigraphic datum); (Matthiessen et al., 2009); Blue (8) = Top Basement (~300 Ma). (B) Depth-converted seismic profile SV-3-97. Grey boxes indicate 1=seabed; 2=2.6 Ma, 3=6.2 Ma, 8=Top Basement (as indicated in (A)), and four reconstructed layers, i.e. 4 = 12 Ma, 5 = 15.2 Ma, 6 = 17.4 Ma, 7 = 18.5 Ma using the age model of ODP Hole 909C (Winkler et al., 2002; Wolf-Welling et al., 1996). The source rock units are defined between layers 5 and 6 from direct observation of ODP Hole 909C (Knies and Mann, 2002) and in layer 7 from inferred deeper located source rocks below the base of ODP Hole 909C (~17.4 Ma) (Stein et al., 1995). Different color codes of the layers indicate variable converted depths (in meters) below seafloor. Blue circles indicate the position of the gas flares in the water column on the eastern VR (Bünz et al., 2012). Notice the location of gas flares at the crest of an anticline characterizing the VR. Site location for ODP Sites 909 and (projected) 986 are given.

ACCEPTED MANUSCRIPT

The main objectives of this study are two-fold: (A) To improve our understanding of the spatial and temporal evolution of the potential hydrocarbon sources in the eastern Fram Strait and (B) to apply a migration modelling approach to better determine the timing of initial onset and duration of methane seepage on the Vestnesa Ridge gas hydrate system and identify the potential controlling factors for this evolution. This region is particularly well-suited for the study of long-term variations of methane seepage because (1) it is located within the spatial and temporal extent of a petroleum system (Dumke et al., 2016; Knies and Mann, 2002); (2) there are known migration pathways through faults and fractures (Plaza-Faverola et al., 2015); and (3) deep carbon sourced gas hydrate formations (Smith et al., 2014) with a prominent bottom simulating reflector (BSR) (Hustoft et al., 2009) exist in regions of extensive gas seepage at the seafloor (Bünz et al., 2012).

2. Data and methods

2.1 Data

The input/calibration data for the hydrocarbon migration modelling were mainly derived from geochemical and sedimentological studies of ODP Sites 909 and 986 from the Atlantic-Arctic gateway region including calculated amounts of marine and terrestrial organic carbon, estimated paleo-productivity, headspace gas data and silt/shale ratio, as well as carbonate contents published by Myhre et al. (1995), Stein et al. (1995), Butt et al. (2000), and Knies and Mann (2002). The basin configuration, derived from the 2D seismic reflection profile SV-3-97, is supported by inferred non-deposition and sub-aerial exposure of ODP Site 908 (Hovgård Ridge) between ~25 and ~6.7 Ma (Matthiessen et al., 2009) in the west, and constant sub-aerial exposure of the Svalbard/Barents Sea platform since the Middle Miocene in the east (Knies and Mann, 2002 and references therein). The details of the basin

configuration as baseline for the hydrocarbon migration model are provided below. The SV-3-97 2D seismic profile was acquired in 1997 using a 4.2 km cable with a towing depth of 9±1 m and an array of sleeve guns at a towing depth of 6 m with a shotpoint interval of 37.5 m. The dominant frequencies of the seismic line are between 12-40 Hz, giving an approximate vertical resolution varying between 15-40 m, depending on depth.

2.2 Petroleum systems modelling

Petroleum system analysis (PSA), a well-established method in hydrocarbon exploration, numerically models processes of hydrocarbon generation, migration, trapping and leakage within sedimentary basins over geological times. For this study, we used the Migri simulator (http://www.migris.no/technology), a fast commercial PSA software toolkit. All modelled properties are treated dynamically, meaning their values change through geologic time. Details on the methods for modelling the individual processes are described in Sylta (2005); we briefly summarize key processes relevant for this study here.

The vertical entry pressure distribution within and between the layers is evaluated to determine whether primary migration out of the source rocks should be directed upward or downward. Over time, entry pressure values in the grid elements are calculated from the permeabilities, which are derived from the lithological composition and burial depths (see "lithology and burial history"). Secondary migration is modelled as mostly buoyancy-driven within permeable systems underneath flow barriers. Commonly, the direction of flow is governed by the steepest gradient of ascent. Lateral entry pressure differences within the flow unit may, however, cause the flow to be deflected. Lateral migration may also be stopped or deflected when the flow encounters a shale pinch-out barrier with higher entry pressures than more porous strata. Migrating hydrocarbons are modelled to accumulate in traps. Gas and

subsequently oil are modelled to leak out of the trap according to the entry pressure distributions modelled in the sealing rocks (e.g. in shales). Both, the trapped hydrocarbon column heights and the seal permeabilities determine the rates and areas of leakage from traps. This PSA approach is well-suited to unravel the hydrocarbon leakage history off the western Svalbard coast towards the Atlantic-Arctic gateway region by placing constraints on the timing of hydrocarbon generation and migration, as well as on the volume of leaked hydrocarbons. We modeled two scenarios with different qualities and thicknesses of a known, gas prone (kerogen type III), Miocene source rock observed in ODP Hole 909C and inferred to be deposited (attaining 70-130 m thickness) prior to late Cenozoic (Plio-Pleistocene time) prograding sequences on the western Svalbard margin (Eiken and Hinz, 1993; Mattingsdal et al., 2014).

2.2.1 Basin model setup

Our petroleum system model is built upon a set of input parameters, whose definitions are outlined below and summarized in Tables 2 and 3. The model is simulated on grid cell sizes of 50 m x 50 m. The vertical model resolution is 30 m on average, but changes in accordance to the vertical lithological variability on sub-meter scale allowing a vertical model resolution down to 10 m. This variable vertical resolution is achieved through a definition of several sub-layers in each stratigraphic unit.

2.2.2 Basin configuration

Three main horizons were interpreted in addition to the seafloor, on the 2D seismic profile SV-3-97 based on correlation to ODP Hole 909C (Fig. 2). These include: Top basement (assigned age of 300 Ma to avoid impact on the basin modelling), the 6.2 Ma regional

biostratigraphic datum for the Nordic Seas and Arctic Ocean (Matthiessen et al., 2009) and the Matuyama/Gauss chron boundary (~2.6 Ma) (Knies et al., 2009; Mattingsdal et al., 2014). The horizons were depth converted using the velocity profile for ODP Site 909 (Myhre et al., 1995):

$$TVD_{Horizon} = (TWT_{Horizon})^2 * 0.00026 + TWT_{Horizon} *0.7 + 4.8 + TVD_{Seabed} \quad (1)$$

and

$$TVD_{seabed} = 1.470 m/s * TWT_{Seabed} * 0.5 \quad (2)$$

where $TVD_{Horizon}$ is the true vertical depth below sea level, $TWT_{Horizon}$ is the two-way travel time of a given seismic reflector and TVD_{seabed} is the true vertical depth of the seabed. TWT_{seabed} is the two-way travel time of the seabed reflector. The average deviation of the depth-converted horizons from their corresponding well tops in ODP Hole 909C is 22 m. The seismic profile SV-3-97 is artificially broadened by adding grid nodes with identical properties perpendicular to the line (artificial width is ~750 m) to create a pseudo 3D model for better handling and visualization (Fig. 2). Three additional layer-bounding horizons were constructed using depth and thickness relations from the ODP Hole 909C stratigraphy. They represent horizons "4-6" in Figure 2 and were assigned ages to the model at 12.0 Ma, 15.2 Ma, and 17.4 Ma, respectively. Two intervals (17.4 Ma, 15.2 Ma) represent source rock units in the model and correspond to organic-rich deposits identified in ODP Hole 909C (Fig. 2) (Knies and Mann, 2002). A fourth horizon (horizon “7” in Figure 2), lithostratigraphically unconstrained, was inserted at an isopach fraction at 25% of thickness below the 6th horizon. This 7th horizon, with an assigned model age of 18.5 Ma defines a deeper, hypothetical source rock, as inferred by Stein et al. (1995). As part of the basin configuration reconstruction, the main interpreted faults on seismic profile SV-3-97 were included in the model (Fig. 2).

2.2.3 Burial history

Burial history reconstruction was performed using a backstripping approach (Allen and Allen, 2005) with paleo-bathymetries inferred to follow present-day marine trends, and water depths to be about 50% of that of present-day. The latter is inferred from a hiatus (sub-aerial exposure) recorded in nearby ODP Site 908 between ~25 and ~6.7 Ma (Matthiessen, 2009) and subtraction of the present-day water depth at ODP Sites 908 and 909, assuming constant tectonically-induced subsidence. Thicknesses and depth of units over time are derived from decompaction using the concept of Sclater and Christie (1980). The permeabilities of the units are calculated dynamically over time and range from impermeable to 7000 mD. They are based on the lithologies and porosity estimates from the decompaction calculation (Table 2). Each interpreted and constructed depth horizon in Figure 2 has an assigned absolute age based on the chrono- and litho-stratigraphic interpretation for ODP Hole 909C (Myhre et al., 1995; Winkler et al., 2002; Wolf-Welling et al., 1996). These ages are from bottom (horizon 8) to top (horizon 1) ~300Ma (oceanic basement), 18.5 Ma, 17.4 Ma, 15.2 Ma, 12.1 Ma, 6.2 Ma, 2.58 Ma and present-day. Based on initial model runs, no significant hydrocarbon generation is modelled before ~10 Ma. Additional model time steps are calculated using linearly interpolated model parameters. Those additional time steps aid in a refined estimation of hydrocarbon maturation, generation, migration and leakage quantification. They have been placed at 7.85 Ma, 4.39 Ma, 1.93 Ma, 1.29 Ma, 0.05 Ma and 0.02 Ma. Consequently, the petroleum systems modelling is performed over total 10 model time steps between 12.1 Ma and present-day (Table 2).

2.2.4 Lithological model

The vertical resolution of the model was fitted to capture the fluctuation of the sand-shale ratios observed in ODP Sites 909 (Wolf-Welling et al., 1996) and 986 (Butt et al., 2000). Depth, age, and lithology information from ODP Hole 986D (Butt et al., 2000; Knies et al., 2009) are projected onto the model's depth-age relation at the Vestnesa Ridge. We expect that Pleistocene, glacially-derived sediments there are more coarse-grained compared to pre-glacial sediments (with age >2.7 Ma) and are comparable with the lithological composition of ODP Hole 986D (Butt et al., 2000). Consequently lithostratigraphic information from ODP Hole 909C (for stratigraphic ages from 17.4 Ma to 2.6 Ma) and the projected ODP Hole 986D (for stratigraphic ages from 2.6 Ma to 0 Ma) were combined to populate the model with a laterally invariant sand-shale-carbonate ratio stratification, between the top basement and the seafloor reflectors. The entire lithological model is stratified according to borehole information and therefore accounts for vertically changing proportions of shale, sand and carbonate (Table 2). Strata with low shale and high sand contents are characterized by higher porosities and permeabilities compared to high shale content strata at a similar burial depth. The former can be regarded as traditional carriers and generally act as conduits for fast, lateral hydrocarbon migration.

2.2.5 Source rock quality and quantity model

Two source rock units were defined in accordance with the findings of two organically enriched and thermally immature siliciclastic intervals in ODP Hole 909C (Myhre et al., 1995) (Table 3). The model for the source rock interval between 17.4 Ma and 15.2 Ma employs laterally variable total organic carbon (TOC) and hydrogen index (HI) values along the profile as predicted by the organic facies distribution model of Knies and Mann (2002) (Fig. 3).

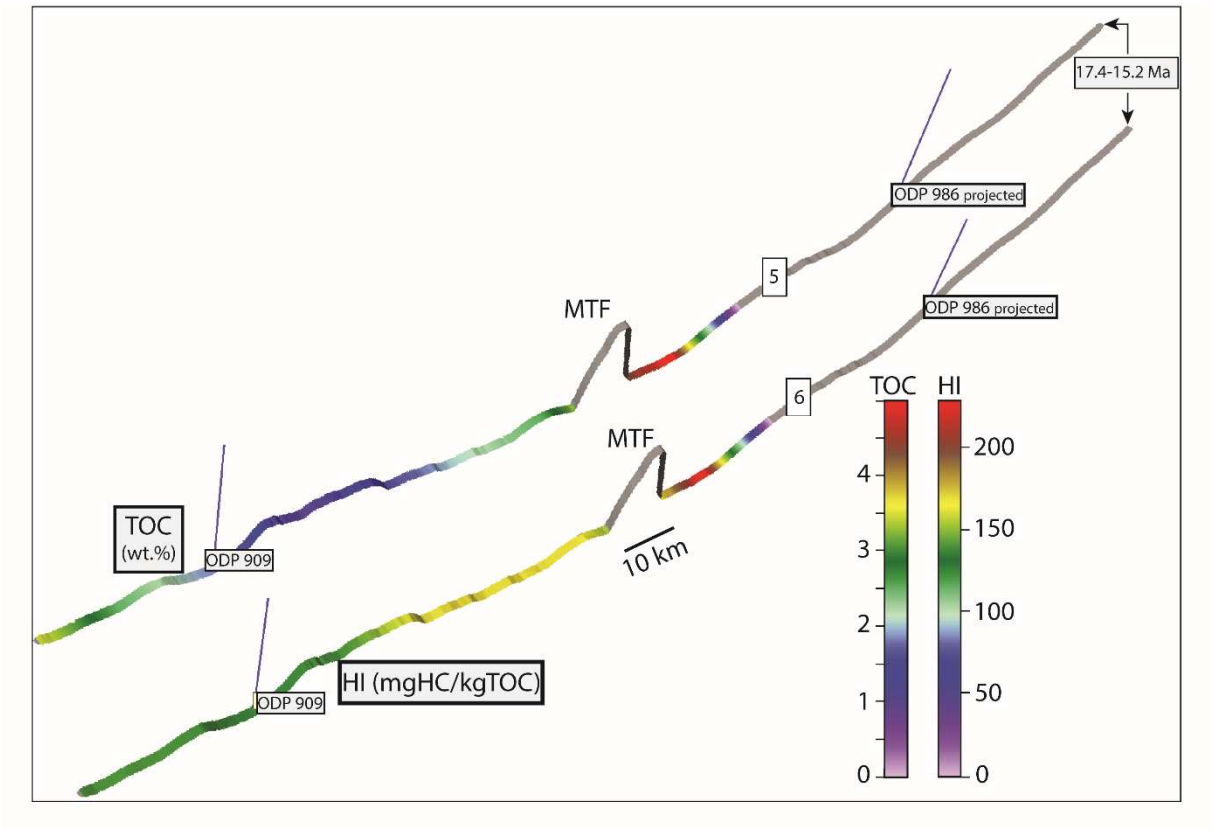

Fig. 3: Source rock characteristics for middle Miocene deposits along seismic profile SV-3-97. The two layers (numbered in Figure 3 as 5 and 6) are constructed using depth and thickness relations from the ODP Hole 909C stratigraphy and added to the model at 17.4 Ma and 15.2 Ma (see main text for further explanations). Total organic carbon (TOC, in wt.%) and Rock Eval Pyrolyses hydrogen index (HI, mgHC/gTOC) in these two stratigraphic layers at 17.4 and 15.2 Ma are derived from direct observations in ODP Hole 909C and laterally modelled by applying the 2D organic facies model outlined in Knies and Mann (2002). Gray intervals = no source rock information.

According to this model, TOC values range from 0 to 5 wt% and HI values span between 20 and 230 mgHC/gTOC (Fig. 3). For the interval between 15.2 Ma and 12.0 Ma, uniform values for TOC of 1.0 wt% and HI of 50 mgHC/gTOC are used, as observed in ODP Hole 909C (Myhre et al., 1995). A third, conceptual Miocene source rock unit was included below the base of ODP Hole 909C (horizon "7" in Figure 2) in order to imitate a potential source for the

migrated hydrocarbons encountered at the base of ODP Hole 909C (Stein et al., 1995). Constant values for TOC of 2 wt%, HI of 100 mgHC/gTOC, and thickness of 50 m are modelled underneath the Vestnesa Ridge, to the northeast of the Molloy Transform Fault (MTF) (Table 3). Type III kerogen kinetic schemes from Behar et al. (1997) are used for the maturation and generation modelling of all three sources (Table 3).

2.2.6 Thermal history model

Our thermal history model assumes the highest geothermal gradients at the MTF location and decreasing gradients away from the MTF in SW and NE directions (Vanneste et al., 2005). Present-day geothermal gradients measured at the ODP Sites 908, 909, 910, and 912 range between 55 °C/km and 88 °C/km (Stein et al., 1995). These geothermal gradients were projected onto the SV-3-97 profile to map their pattern along the profile (Fig. 4). A maximum geothermal gradient of 150 °C/km is assumed at the centre of the MTF, in accordance with published inferences of Dumke et al. (2016), Hustoft et al. (2009), and (Smith et al., 2014). Measured and assumed geothermal gradient values are consistent with reported heat flow values of Hustoft et al. (2009) and Smith et al. (2014) west of Svalbard, considering thermal conductivities of silt-shale lithologies. In the absence of constraints on the thermal history, we employ the present-day gradient setting for all model time-steps. Figure 4 shows the inferred gradient distribution along strike of seismic profile SV-3-97. A seabed temperature distribution at present-day is plotted along the profile and is based on temperature-depth patterns observed along the western Svalbard margin (Dumke et al., 2016; Johnson et al., 2015; Rajan et al., 2012; Smith et al., 2014) and observed values available in the World Ocean Database (WOD, 2013). Due to the high geothermal activity at the MTF location, we infer a slightly higher seafloor temperature there (3 °C). This has, however, little effect on the model. Furthermore, high sedimentation rates during Pliocene/Pleistocene times at the

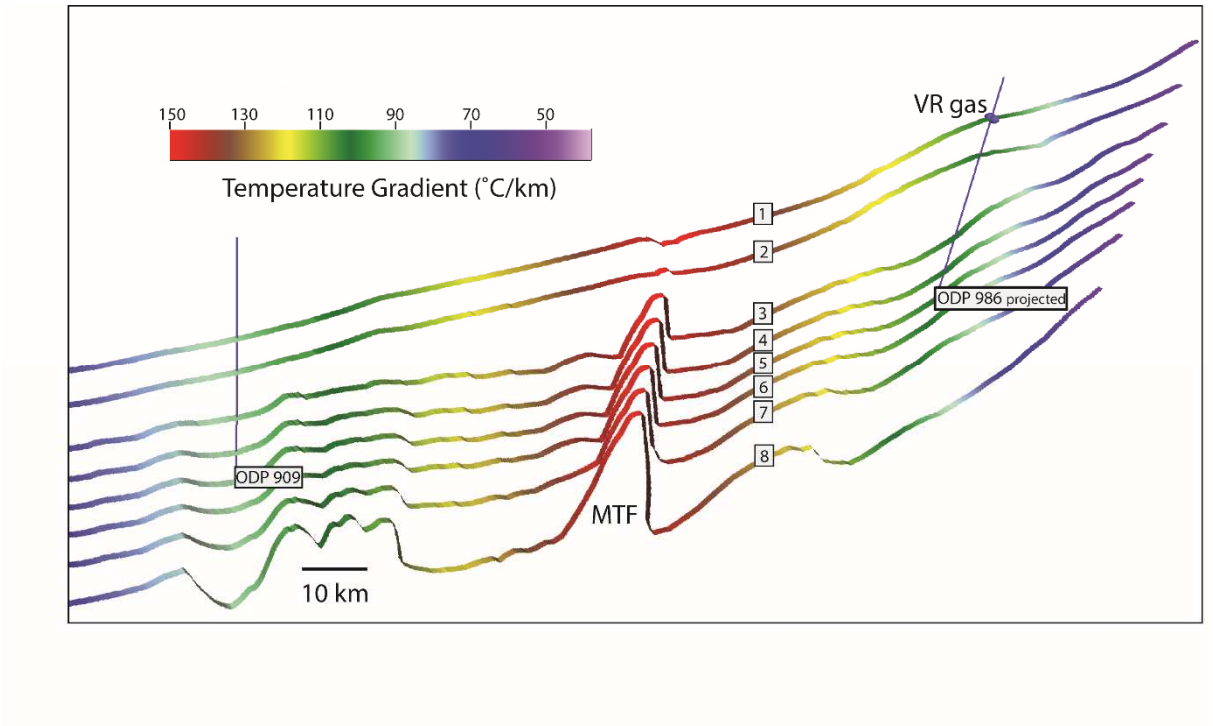

Fig. 4 Geothermal gradient for sediment sequence along seismic profile SV-3-97. Measured gradients in ODP Sites 909 and 986 (55-88 °C/km) are projected onto SV-3-97. Highest gradients are assumed to occur at the MTF with values of max. 150 °C/km (Dumke et al., 2016).

Vestnesa Ridge exerted a cooling effect in the upper sedimentary layers (Plaza-Faverola et al., 2017). The resultant transient changes in the thermal regime challenge the assumption of a constant geothermal gradient over time and, hence, impact the correct approximation of the timing of source rock maturation. To account for this, we use the equation of Palumbo et al. (1999) to locally evaluate the thermal impact of the rapid sedimentation on the timing of the source rock maturation.

2.2.7 Organic matter maturation

Vitrinite reflectance measurements within the source rock units (ODP Hole 909C) range from 0.4%Ro (12.0 Ma) to 0.5%Ro (17.4 Ma) and indicate an immature to marginally mature

thermal status of the units (Knies and Mann, 2002). Our thermal and burial history model at the borehole location fits these measurements when applying the vitrinite model of Burnham and Sweeney (1989a, 1989b) (Fig. 5).

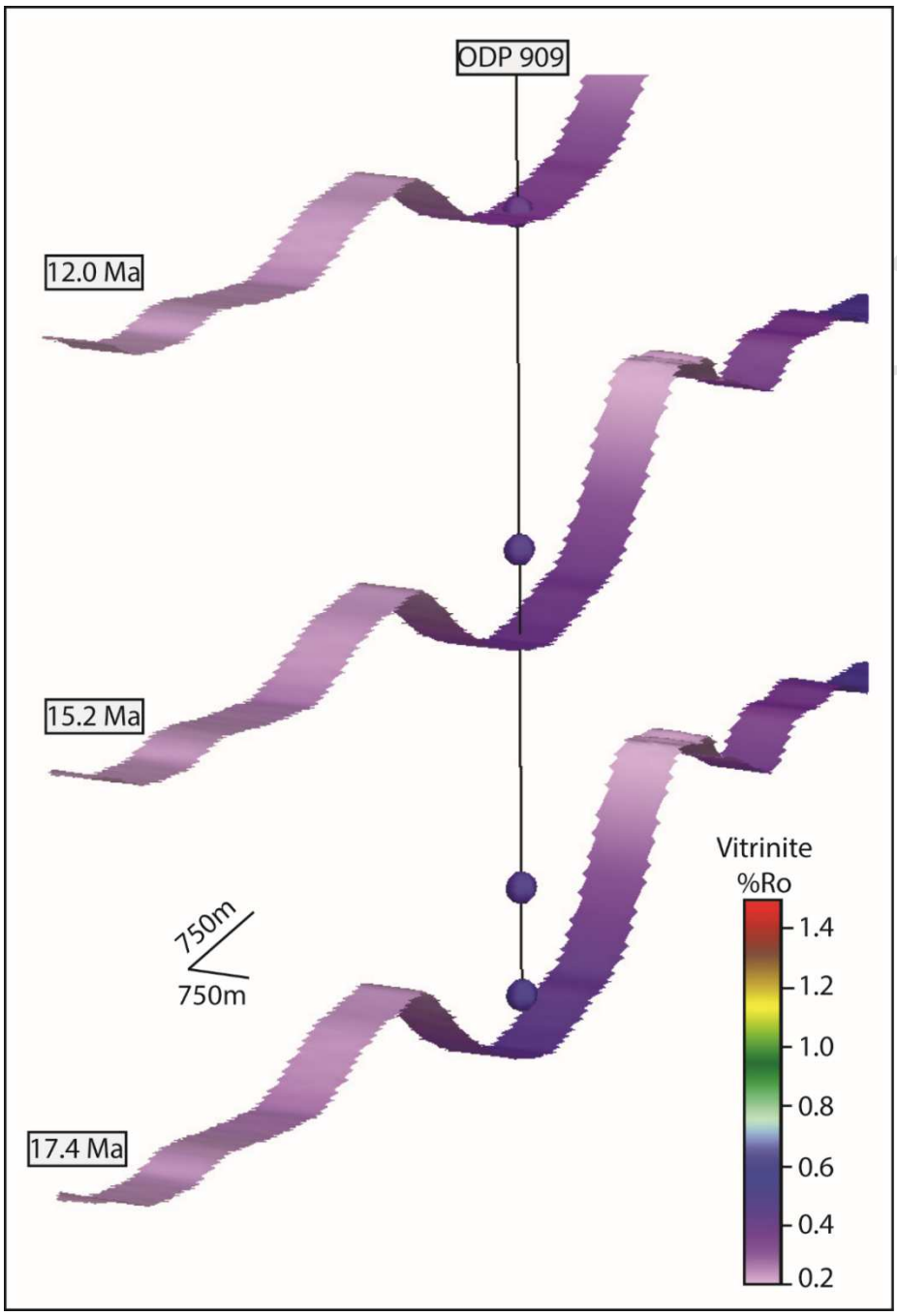

Fig. 5 Modelled vitrinite reflectance maturities of the Middle Miocene source rock for three time steps during the middle Miocene directly in the vicinity of ODP Hole 909C (top: 12.0 Ma, centre: 15.2 Ma, base: 17.4 Ma). Superimposed are the vitrinite reflectance measurements within ODP Hole 909C (colored circles).

Hydrocarbon saturations of less than 5 ppm are recorded within the two source rock units between 12 and 17.4 Ma (horizons "4-6" in Figure 2) in ODP Hole 909C (Myhre et al., 1995; Stein et al., 1995), while a significant increase (5 to 10 fold) of hydrocarbon saturation occurs at the base of the borehole. These hydrocarbon concentrations led to the inference that, based on the low maturity state of those source rocks, migration from a deeper allochthonous gas source must account for the high hydrocarbon concentrations at the base of Hole 909C (Stein et al., 1995). In our model, this is represented by the third conceptual Miocene source rock (horizon "7" in Figure 2). For the modelled source rock maturation, our generation model estimates a bulk hydrocarbon concentration of less than 2ppm for the lower source rock unit (horizon “6” with an age of ~17.4 Ma), and thus, we infer a good model calibration at the location of ODP Hole 909C for both the thermal and burial history as well as the hydrocarbon generation model.

3. Chronology and basin evolution

The chronostratigraphic framework in Hole 909C indicates the recovery of a complete Middle Miocene sequence, with the age model revealing a variable sedimentation rate (3-15 cm/kyr) (Wolf-Welling et al., 1996). Central for the modelling are paleomagnetic and biostratigraphic ages at ~2.6 Ma (181.8 mbsf, Matuyama/Gauss chron boundary) and ~6.2 Ma (657 mbsf, last appearance of acritarch *Decahedrellla martinheadii*) (Matthiessen et al., 2009). These chronostratigraphic horizons are correlated across the eastern Fram Strait with high-resolution 2D seismic data (Fig. 2). The organic-rich rocks at the base of ODP Hole 909C were likely deposited prior to 15 Ma (Knies and Mann, 2002). Seismic interpretation of the seafloor and top oceanic basement complete the configuration of the basin (Fig. 2). The basin evolved during the opening of the Fram Strait in the early Oligocene (33 Ma) and the subsequent development of the ultraslow-ocean-spreading Molloy and Knipovich ridges. Both ridges are

offset by the Molloy Transform Fault (Fig. 1). From the opening of the Atlantic-Arctic gateway (~17 Ma) (Jakobsson et al., 2007) to ~2.7 Ma, the basin was filled with fine-grained sediment drift deposits (silty-clay); since 2.7 Ma, a larger component of glacially-derived sands (30-74 % portion) filled the basin (Butt et al., 2000; Knies et al., 2009). These sedimentary sequences are incorporated in the model. Modelled geothermal gradients are kept constant throughout the evolutionary phase of the basin (Fig. 4) with highest values of 150°C near the MTF, and lowest values of ~50°C on the Vestnesa Ridge in the east and around ODP Site 909 in the west. This leads to higher maturity levels (oil window at ~0.5 vitrinite reflectance) of organic-rich deposits near the MTF location and towards the Svalbard Platform as rapid burial due to higher sedimentation rates took place (Fig. 4). Indeed, the deepwater hydrated sediments at the Vestnesa Ridge, a >100-km-long and 50-km-wide, at least 17 Ma old sediment drift (Mattingsdal et al., 2014), are located on hot (100-150 mW m^{-2}) (Crane et al., 1991) and young (<20 Ma) oceanic crust created at the Molloy Ridge (Fig. 1) (Engen et al., 2008). These sediments comprise a methane reservoir of 0.5-0.9 Gt (Hustoft et al., 2009). Charged by a mix of shallow biogenic and deeper thermogenic gas sources, free gas bypasses the gas hydrate stability zone (GHSZ) via near-vertical faults and fractures (Plaza-Faverola et al., 2015) and contributes to the presently active seepage system on the ridge (Bünz et al., 2012; Plaza-Faverola et al., 2017; Smith et al., 2014). Although the rates of gas flux are still unconstrained, observations nearby indicate methane concentration in bottom waters exceeding 100 nM (Steinle et al., 2015) and of mixed origin (microbial/thermogenic) (Knies et al., 2004; Sahling et al., 2014). Sedimentation rates inferred from borehole data (ODP Sites 909 and 986) are an order of magnitude higher along the western Svalbard margin compared to the deep basins in the central Fram Strait (Knies et al., 2009).

4. Results

4.1 Maturation and migration history of thermogenic gas sources in the eastern Fram Strait

Modelling results corroborate empirical observations (Stein et al., 1995) that the main Miocene source rock in ODP Site 909 is thermally immature for hydrocarbon generation. Vitrinite reflectance maturities within the source rock intervals vary between 0.4 and 0.5 (Fig. 5) implying that the gas-window has not been reached for the identified Miocene source rock in the southwestern part of the basin around ODP Site 909 (Stein et al., 1995). Instead, the prime generation area with continuous source maturation is northeast of the MTF with a present maximum burial depth of 4.3 to 4.8 km below sea level and high geothermal gradients between 100 and 130ºC/km (Crane et al., 1991; Dumke et al., 2016). Our modelling suggests that hydrocarbon generation and migration started during the late Miocene (~6.3 Ma) because of the presumed high heat flow near the MTF (today up to 155 mW m^{-2}) (Crane et al., 1991) (Fig. 6). Downslope of Vestnesa Ridge, in areas with the highest Cenozoic sedimentation rates, the transient cooling effect of rapid sedimentation (Palumbo et al., 1999) delays the source rock maturation by ~2 Ma. From the modelling we infer an onset for hydrocarbon generation and migration there between ~6.3 Ma and ~4 Ma. Subsequently, the source rock maturation and hydrocarbon generation front progressed northeastwards towards the Vestnesa Ridge (Fig. 6) because of progressive burial to the northeast of the MTF.

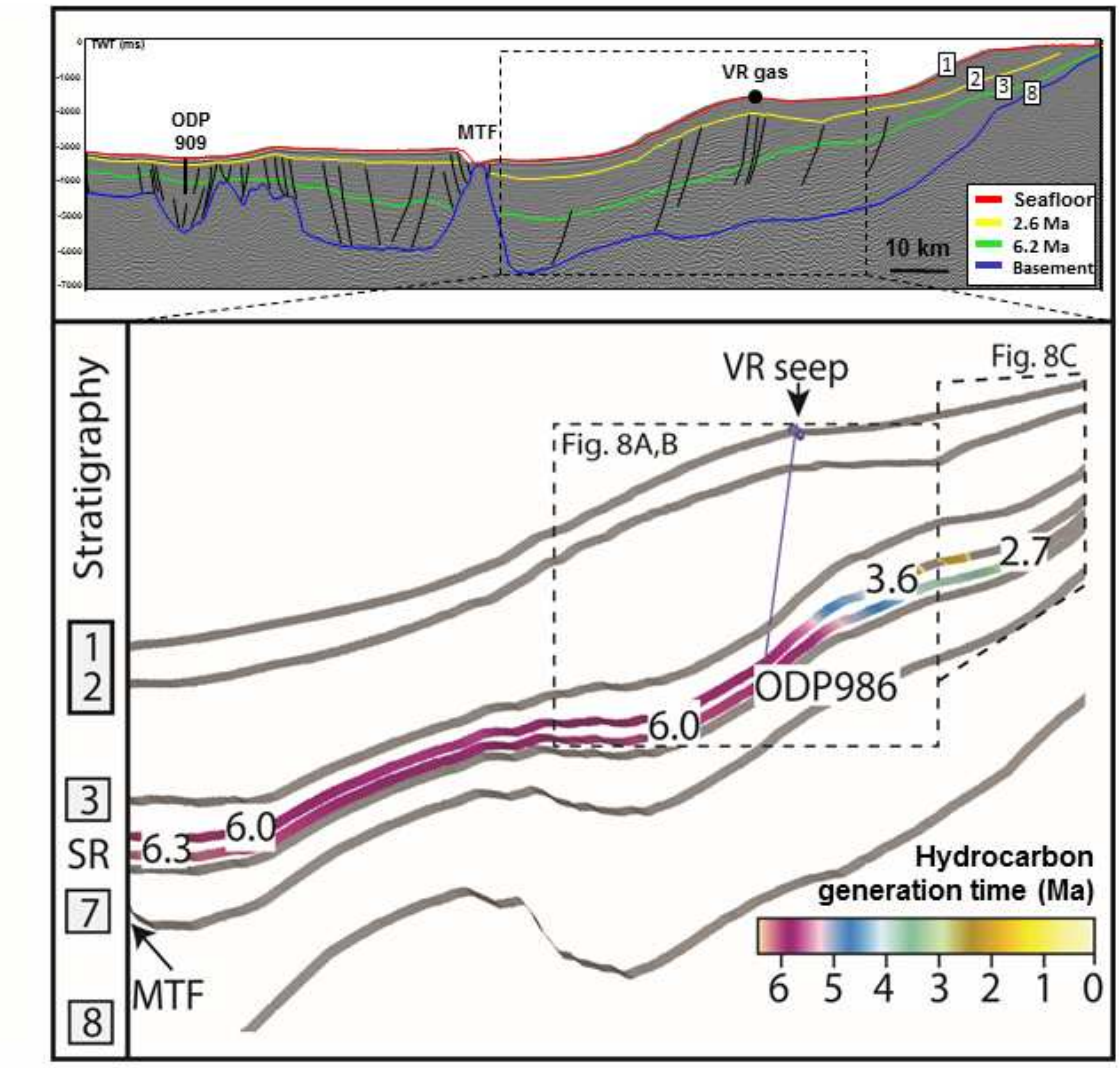

Fig. 6 Timing of hydrocarbon generation along part of a transect SV-3-97 east of Molloy Transform Fault (MTF) towards the western Svalbard margin (see rectangle on seismic line for exact location of the generation and migration model). Different color coding indicates various time periods (in Ma) of hydrocarbon generation within the source rock layers. Note the onset of hydrocarbon generation from Middle Miocene source rock close to MTF at ~6.3 Ma. The stratigraphy, numbered 1-8 is detailed in Figure 2.

The timing for hydrocarbon generation in our study differs from the ages given by Dumke et al. (2016) of 14-10 Ma. This is most likely due to: (a) the improved chrono- and litho-stratigraphic framework, as well as organic facies prediction model of the current study applied to the hydrocarbon potential of the Miocene source rock, and (b) the absence of an inferred Eocene source rock in the Fram Strait in contrast to the findings from central Arctic Ocean (Lomonossov Ridge) (Mann et al., 2009; Stein et al., 2006). The latter is rather controversial since industry wells from the western Barents Sea do not show any evidence for Eocene source rocks in the study region (Ryseth et al., 2003). However, we cannot rule out the possibility that organic-rich (TOC >2 %) sediments recorded in the Central Basin on Spitsbergen during the Paleocene-Eocene Thermal Maximum (PETM) (Dypvik et al., 2011; Riber, 2009) are more widespread, and could have contributed to the expulsion of hydrocarbons upon maturation at an earlier stage than the modelling results indicates. Based on the available observational constraints in the Arctic-Atlantic gateway, the migration model suggests that, since the late Miocene (~6.3 Ma), source rock maturation and eventually hydrocarbon generation occurred progressively upslope and accelerated further after the intensification of the Northern Hemisphere glaciation at ~2.7 Ma due to higher sedimentation rates (Mattingsdal et al., 2014) and rapid burial (Fig. 6).

By modelling the hydrocarbon flow in the two latest time steps (2.0 Ma, 0 Ma) (Figs. 7A, B), we show that lateral and eventually vertical migration is largely dependent on stratigraphic and lithological factors (i.e. permeability), as well as basin topography. Lithological units with low shale content act as conduits permitting lateral hydrocarbon migration from the site of generation (near the MTF) upslope to the Vestnesa Ridge. There, traps are filled and vertically leak gaseous hydrocarbons into shallower stratigraphic levels and towards the sea floor.

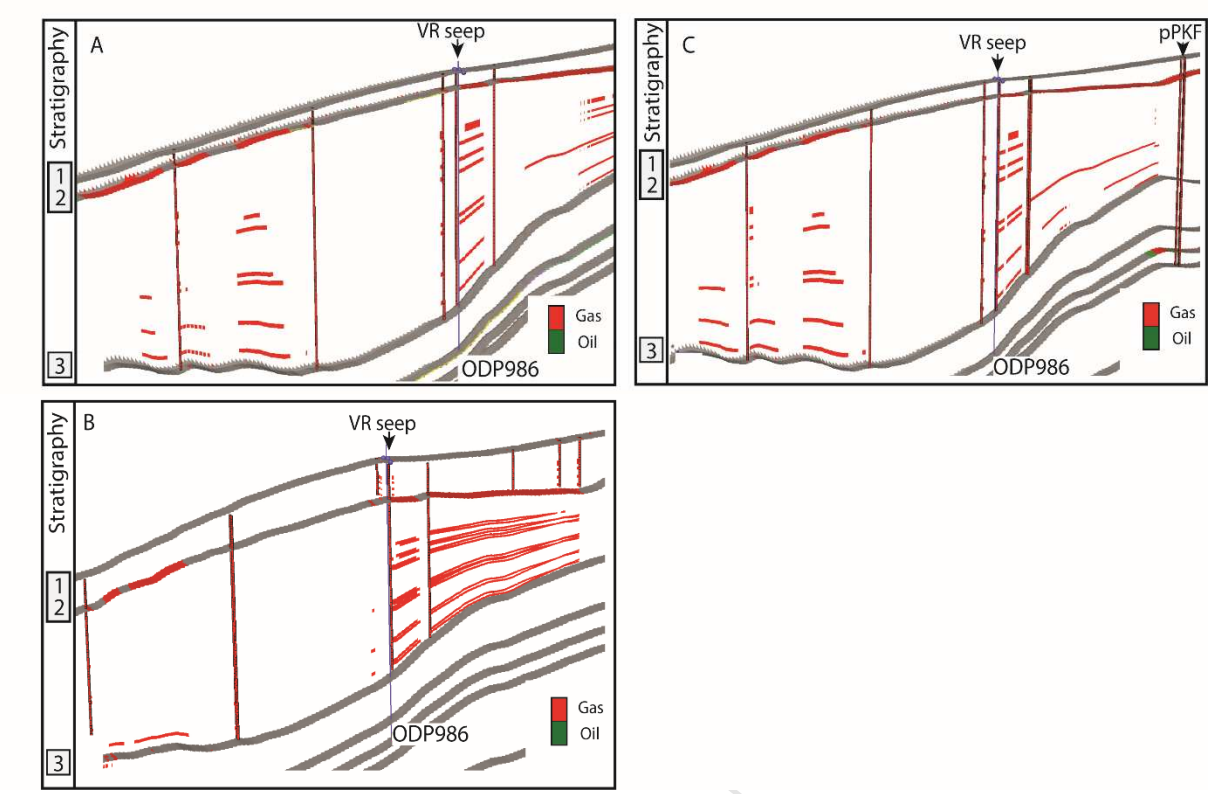

Fig. 7 Modelling of hydrocarbon migration through: (A) Miocene-early Pleistocene sediment sequence at ~2.0 Ma charged by Miocene source rock (SR) of 70 m thickness. (B) at present-day. Note the northeastward migration towards shallower shelf setting. (C) Miocene-early Pleistocene sediment sequence at ~2.0 Ma charged by Miocene source rock of 130 m thickness. Note the migration of hydrocarbon upslope towards the position of the projected gas flares off Prins Karls Forland (PKF). Vestnesa Ridge (VR) seep site and projected position of ODP Site 986 are shown on each figure. The stratigraphy, numbered 1-3 is detailed in Figure 2.

Initial hydrocarbon migration model testing to account for the identified larger (open) faults as potential pathways (Fig. 2), indicates no significant effect on vertical migration of hydrocarbons from primary generation areas to shallow depths. This insensitivity is related to the high permeability values of the sedimentary packages. Permeabilities of up to 7000 mD in

these lithological units facilitates a rapid vertical migration and leakage towards the seafloor. Highest permeabilities are encountered in sand dominated lithologies at shallow burial depths in the model. However, final migration pathways towards the seabed and, consequently the seepage dynamics at the seafloor are certainly controlled by the interconnected fault pattern in shallower strata (Plaza-Faverola et al., 2015; Plaza-Faverola et al., 2017). A detailed fault modelling setup is required to follow the vertical migration pattern towards the seafloor. This is currently beyond the scope of our model, and will therefore be elaborated in a follow-up study.

Our modelling results indicate that around 2 Ma, primarily gaseous hydrocarbons entered, the ~2 km-thick sedimentary package of late Miocene-Pleistocene age below the proto-Vestnesa Ridge by vertical and buoyancy-driven migration (Fig. 7A). Within these sandy, more porous strata, migration continued up-dip along the strata towards the crest of the Vestnesa Ridge and formed local gas accumulations. Eventually hydrocarbons trapped at the crest of the ridge leaked to the paleo-seafloor where clusters of pockmarks with currently active seepage have been documented (Fig. 7B) (Bünz et al., 2012). This hydrocarbon migration-leakage history, which is largely controlled by the structural configuration below the Vestnesa Ridge, does not significantly change if considering an inferred deeper source rock (Fig. 7C) (Stein et al., 1995). However, a thicker (~130 m thickness), and thus more prolific source rock along the entire transect (label "7" in Figure 2) yields: (1) an increased bulk amount of hydrocarbons, (2) hydrocarbons charged into middle Miocene age sandy, porous strata by 2 Ma, and (3) facilitates migration, with trapping and leakage northeast of the Vestnesa Ridge, closer to the Svalbard coastline (Fig. 7C). The larger volumes of hydrocarbons added to the system cause higher pore space saturation and migration efficiency, and thus facilitate a much longer eastward migration distance.

5. Discussion

5.1 A long-term source of thermogenic gas to sustain gas hydrate and seepage along the Vestnesa Ridge

The final opening of the Fram Strait during the late Miocene (Jakobsson et al., 2007; Knies et al., 2014) resulted in the development of a >2 km thick sediment accumulation at the Vestnesa Ridge, as a consequence of extensive ocean current exchange between the Arctic and the North Atlantic (Vogt et al., 1994). Mattingsdal et al. (2014) showed that the depositional environment in the region was dominated by contourites, sourced primarily by the northward flowing West Spitsbergen Current. In addition, products of erosional processes on the emerged Svalbard Platform and the Barents Sea were transported in the adjacent sediment cascade system (Hjelstuen et al., 1996; Knies and Gaina, 2008). This included high amounts of organic assemblages (pollen, spores, plant debris) of fresh terrigenous origin (Boulter and Manum, 1996; Poulsen et al., 1996). With the ongoing deepening and widening of the basin, subsidence and burial of the sediments created a prolific Tertiary petroleum system, with terrigenous-derived, organic-rich, Middle Miocene deposits as the main source rock (Knies and Mann, 2002). Initial hydrocarbon generation at ~6.3 million years ago as documented in Figure 7 was a consequence of the high heat flow near the MTF at 2.2 km burial depth. The timing of initial hydrocarbon generation is significantly younger (by 6 to 8 million years) than previously reported in the area by Dumke et al. (2016). Based on available heat flow measurements in the study area (Crane et al., 1991; Dumke et al., 2016), constant geothermal gradients from the center of the MTF (150 °C/km) towards the basin margins (50-80°C/km) were used throughout the entire modelling interval. This resulted in the onset of hydrocarbon formation to the east of the MTF during late Miocene. The catagenesis of these organic-rich deposits at the MTF (Fig. 8) resulted in hydrocarbon generation and migration,

and thus the necessary prerequisite for thermogenic gas hydrate formation (Panieri et al., 2017; Smith et al., 2014).

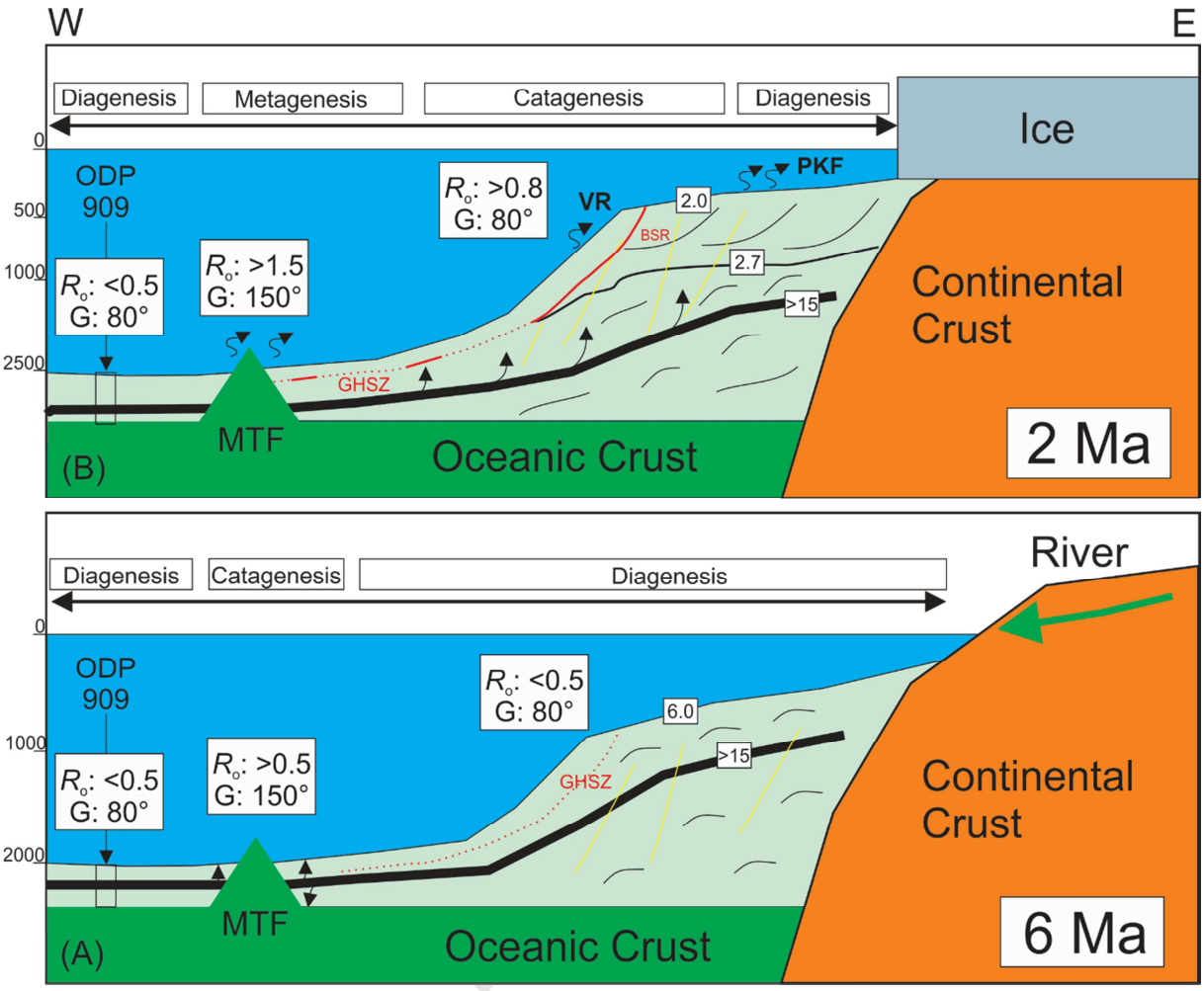

Fig. 8 Schematic illustration for modeled hydrocarbon generation and migration history along the western Svalbard margin. (A) Deposition and burial of Miocene source rocks (>15 Ma) and initial hydrocarbon generation near the Molloy Transform Fault (MTF) around 6 Ma. The inferred source rocks are still too immature (Vitrinite Reflectance Ro <0.5) and geothermal gradients (G) too low (~80ºC/km) to initiate hydrocarbon generation west and east of the MTF. Due to elevated geothermal gradients (~150 ºC/km) near the MTF, organic matter is slightly more mature (Ro >0.5) resulting in initial formation of hydrocarbons. (B) With the intensification of Northern Hemisphere glaciation (~2.7 Ma) and associated high sedimentation rates and rapid burial, further hydrocarbon generation upslope and vertical

migration of hydrocarbons towards the seabed west off Svalbard occurred since 2 Ma. Organic matter near the MTF is overmature for hydrocarbon generation. Patchy BSR east of MTF is likely the result of less generation and thus less vertical migration of hydrocarbons in the deeper part of the continental slope due to metagenesis. Note the low maturity throughout the sequence at the location of ODP Site 909. VR: Vestnesa Rige, PKF: Prins Karls Forland, BSR: Bottom Simulating Reflector, MTF: Molloy Transform Fault, GHSZ: Gas hydrate stability zone. Numbers in white rectangle are surfaces in millions of years. Vertical scale for paleo-bathymetry on the left is in meters. Vertical lithological thickness below seafloor is not to scale.

Through lateral and vertical migration of gaseous hydrocarbons from their kitchen near the MTF, free (thermogenic) gas reached the sub- seabed below the Vestnesa Ridge for the first time ~2 Ma ago. This implies that the gas hydrate system offshore Svalbard was formed coincidentally with the intensification of the Svalbard/Barents Sea continental-shelf-edge glaciations (Mattingsdal et al., 2014) and corroborates recent inferences on multiple seepage events on Vestnesa Ridge over the last 2.7 Ma (Plaza-Faverola et al., 2015). It also supports the timing (~2 Ma) of gas-charged sediment drift formation south of Molloy Ridge (Johnson et al., 2015). Furthermore, it provides a maximum time estimate for the onset of methane release from the seabed into the ocean (Fig. 8). In that sense, the presence of gas hydrates in the region is more a consequence rather than a cause of fluid migration and seepage.

5.2 Implications for explaining seepage regionally offshore western Svalbard

With increased sedimentation rates and rapid burial after the intensification of Northern Hemisphere glaciation at 2.7 Ma, key zones generating and expelling hydrocarbons advanced eastwards (Fig. 8), coinciding with the northward projected location of an active seabed gas expulsion system of thermogenic origin off western Prins Karls Forland (PKF) (Berndt et al.,

2014; Knies et al., 2004; Mau et al., 2017; Portnov et al., 2016; Westbrook et al., 2009). The region also crosses the prolongation of the Hornsund fault zone, a NW-SE striking regional fault system on the western Svalbard shelf (Faleide et al., 1996; Mau et al., 2017). This fault system may be a natural migration pathway allowing the gaseous hydrocarbons of thermogenic origin to bypass potential gas hydrate layers in the sediments. By increasing the source rock thickness in the model by 50 m to accommodate the inferred deeper source rock below the base of ODP Hole 909C (Stein et al., 1995), the modelled active petroleum system could feed the free gas/hydrate formation upslope (Figs. 7C, 8) where gas flares occur at the landward termination of the gas hydrate stability zone (Westbrook et al., 2009). Our model results suggests that methane seepage off western Svalbard likely began millions of years earlier than inferred by U-Th dating of methane-derived authigenic carbonates (MDAC) in the PKF region (Berndt et al., 2014). The latter is supported by the discovery of methane-derived authigenic carbonates (6 and 20 m below seafloor) in the study region in 6 and 20 m depth below seafloor (Bohrmann et al., 2017) suggesting episodic seepage event at least prior to the last glacial period (Panieri et al., 2016; Sztybor and Rasmussen, 2017). Furthermore, from the modeling results we infer that active leakage has been sustained by deeply buried source rocks prone to hydrocarbon generation driven by a combination of rapid burial and high heat flow. The ongoing structurally controlled migration of hydrocarbons from the active petroleum system buried deeply at the Vestnesa Ridge basin have driven and sustained seafloor seepage across the western Svalbard margin over the last 2 Ma. The arrival of large amounts of thermogenic gas to the near-surface at discrete locations determined by the basin structure and migration pathways predicted by our model, adequately explains the restricted character of seepage to this region as observed today (Bünz et al., 2012). The retreat of the ice sheet and the regional stress regime are the main external mechanisms controlling seepage at these currently active cold seep sites (e.g. Portnov et al., 2016; Plaza-Faverola et al., 2015).

5.3 Implications for estimating gas fluxes to the ocean

Analogous to venting gas through the GHSZ in subsurface petroleum systems of the Gulf of Mexico (Sassen et al., 2001), our results imply a strong link between the underlying, thermogenic petroleum system and the present-day seep/gas hydrate activity. Estimates of hydrocarbon flow to the seabed over the last 2 Ma ranges from 0.4 to 4 10^9 m^3 (0.55 to 5.5 m^3/day), which is equivalent to 0.45 to 4.5 nMol/l (Table 4). For an assumed leakage site of 50 m x 50 m, the modelled leakage rates to the seafloor translate into average methane flux rates of 0.58 to 5.76 kg/m^2 per year. This coincides well with inferred methane flux rates of 0.96 kg/m^2 to enable methane bypassing the GHSZ via chimneys in sandy-silty lithologies comparable to those identified off western Svalbard (Butt et al., 2000; Liu and Flemings, 2007). Potential addition from abiotic methane generated from serpentinized ultramafic rocks as proposed for the central/southern Knipovich Ridge (Rajan et al., 2012) and along large detachment faults south of the MTF (Johnson et al., 2015), is not very likely beneath Vestnesa Ridge due to: (a) the configuration of the reconstructed basin where sedimentary units pinch-out towards the MTF (Fig. 2), which excludes migration of any potential abiotic methane towards Vestnesa Ridge, (b) isotopic evidence in Vestnesa Ridge gas hydrate samples showing no evidence for methane produced by serpentinized ultramafic rocks (Panieri et al., 2017; Plaza-Faverola et al., 2017; Smith et al., 2014), and (c) the inferred age and temperature of oceanic crust beneath Vestnesa likely incompatible with recent abiotic methanogenesis (Johnson et al., 2015; Dumke et al., 2016).

Given the present-day subsidence and burial rates near the MTF location with constant high heat flow (~150 °C) and modeled vitrinite reflectance of >1.5%Ro (Fig. 8), a critical state of source rock maturation (metagenesis) for gas and oil formation has been reached northeast of the MTF. This potentially explains the low volume of hydrocarbons currently generated and migrated west of Vestnesa Ridge and downslope (Fig. 7B). In contrast, potential Middle

Miocene source rocks deposited further upslope and on the shelf region have just reached the oil/gas generation window (catagenesis) (Fig. 8). This implies a shorter geological lifetime of the petroleum system for hydrocarbon generation in the deeper part of the continental slope compared to the shelf region (e.g. around PKF). This may explain the strong variability of gas expulsion at the seabed on Vestnesa Ridge (Bünz et al., 2012) compared to the more active cold-seep system further upslope off PKF (350-400 m isobaths) (Mau et al., 2017; Sahling et al., 2014; Steinle et al., 2015; Westbrook et al., 2009). It may also explain the inconsistency of the BSR downslope (Hustoft et al., 2009) because of low hydrocarbon generation potential of the overmature source rock in the basin center today and thus less vertical hydrocarbon flow to the seafloor (Fig. 8).

6. Conclusions

For one of the most active, submarine cold seep systems in the Arctic, we implemented a basin modelling approach to constrain the timing of thermogenic gas generation and migration from deep operating petroleum systems to the gas hydrate and associated seepage system on Vestnesa Ridge, offshore western Svalbard. Our modelling results lead to the following main conclusions:

- The petroleum system below the cold-seep system off western Svalbard down to ~2000 m water depth has been active for the last ~6 million years and frequently charged the seafloor with migrating hydrocarbons ~4 million years later until today.
- The heterogeneity and variable burial depth of the potential Middle Miocene source rocks are the main controls on this operating petroleum system. The structurally controlled accumulation and migration history of thermogenic gas in shallow strata has sustained seepage in regions influenced by ice-sheet dynamics and tectonic stress.

- A thermogenic source rock between the west-Svalbard shelf break and the mid-ocean ridges may have provided the necessary gas to sustain seepage at Vestnesa Ridge, and probably off the coast of Prins Karl Forland since the intensification of Northern Hemisphere glaciations, ~2.7 Ma.
- Independent of past warm-cold climate cycles during the Pleistocene, the hydrate system off western Svalbard has been continuously fueled by deeply buried terrestrial carbon, implying that recent gas hydrate instabilities are superimposed effects on long-term natural leakages.

ACCEPTED MANUSCRIPT

Acknowledgments

This research used samples and data provided by the International Ocean Discovery Program (IODP), in addition to seismic profile SV-3-97 provided by the Norwegian Petroleum Directorate (NPD). This research is part of the Centre of Excellence "CAGE - Arctic Gas Hydrate Environment and Climate" (RCN grant 223259) and Petromaks2 NORCRUST (RCN grant 255150). Stephen Anthony Clark and Alun Hubbard improved an earlier version of the manuscript. The authors acknowledge funding from Statoil ASA, Lundin Norway AS, and Eni Norge AS.

ACCEPTED MANUSCRIPT

Table 1: Applied Ocean Drilling Program (ODP) borehole information for the basin modelling

Borehole	Longitude	Latidude	Water Depth
ODP 910A	80°15.882 N	6°35.405 E	556.4 m
ODP 911A	80°28.466 N	8°13.640 E	901.6 m
ODP 912A	79°57.557 N	5°27.360 E	1036.8 m
ODP 909C	78°35.096 N	3°4.222 E	2519 m
ODP 908A	78°23.112 N	1°21.637 E	1273.6 m
ODP 986C	77°20.431 N	9°04.664 E	2051.5 m
ODP 986D	77°20.408 N	9°04.654 E	2051.5 m

Table 2: Basin modelling input parameters

Parameter / variable	Units or dependance	Physical meaning	Reference
Spatial resolution	50 m x 50 m	Area represented by a grid cell	
	10 - 30 m $n_{sublayer}$-dependent	Height of a grid cell	
$N_{horizon}$	Total 8 4 from seismic interpretation 4 constructed from seismic horizon- and well-data	Number of depth horizons used to construct the model layers	
$N_{sublayer}$	2 - 55 layer thickness and lithological variation dependent	Number of discrete lithological subunits in a model layer	
N_{time}	10 between 12.1 Ma and 0 Ma	Number of model time steps	
dT/dz	55 - 150 °C km^{-1} location-dependent along the profil	Geothermal gradient	Hushoft et. al, 2009, Johnson et al., 2014, Smith et al., 2014, Stein et al., 1995
V_{sh}, V_{ca}, V_{ss}	0 - 1	Fraction of shale, carbonate and sand $V_{sh} + V_{ca} + V_{ss} = 1$	
ϕ	0.09 - 0.59 lithology- and depth-dependent	Porosity fraction (minimum value range for all cells)	
K	10^{-7} - $7 \cdot 10^{3}$ mD lithology- and depth-dependent	Permeability	
P_c	10^{-2} - $1.7 \cdot 10^{2}$ MPa hydrocarbon phase- and K-dependent	Capillary pressure (maximum value range for all cells)	

Table 3: Input model parameters for 3 source rock units

Parameter / variable	Units or dependance	Physical meaning	Reference
Source rock unit I age: 17.4 - 15.2 Ma			
TOC_0 [I]	Up to 5 wt%,	Total organic carbon in the source I prior to thermal alteration	Knies and Mann, 2002 Stein et al., 1995
HI_0 [I]	20 - 230 mgHC $gTOC^{-1}$	Initial hydrogen index of kerogen in source I prior to thermal alteration	Knies and Mann, 2002 Stein et al., 1995
Thickness [I]	Up to 223 m	Effective thickness of source I	Knies and Mann, 2002 Stein et al., 1995
Source rock unit II – age: 15.2 - 12.0 Ma			
TOC_0 [II]	1 wt%,	Total organic carbon in the source II prior to thermal alteration	Stein et al., 1995
HI_0 [II]	50 mgHC $gTOC^{-1}$	Initial hydrogen index of kerogen in source II prior to thermal alteration	Stein et al., 1995
Thickness [II]	Up to 155 m	Effective thickness of source II	Stein et al., 1995
Source rock unit III – 18.5 Ma; Vestnesa Ridge only			
TOC_0 [III]	2 wt%,	Total organic carbon in the source III prior to thermal alteration	
HI_0 [III]	100 mgHC $gTOC^{-1}$	Initial hydrogen index of kerogen in source III prior to thermal alteration	
Thickness [III]	50 m	Effective thickness of source III	
Source rock characterization			
kerogen type [I, II, III]	Terrigenous, type III	Kerogen type of organic matter	Stein et al., 1995
kinetic scheme [I, II, III]	Behar type III	Kinetic scheme for the kerogen to hydrocarbon transformation for all source rocks I, II, III	Behar et al., 1987

Table 4: Properties for methane flux estimates

Parameter / variable	Units or dependance	Physical meaning	Reference
Methane properties			
$M_{methane}$	16.04 g mol^{-1}	Molar mass of methane	
$\rho_{methane}$	0.72 kg m^{-3}	Density of methane at 0 °C and 1013HPa	GESTIS database http://gestis-en.itrust.de

References

Allen, P.A., Allen, J.R., 2005. Basin analysis - Principles and Applications, 2nd edition ed. Blackwell Publishing Ltd.

Behar, F., Vandenbroucke, M., Tang, Y., Marquis, F., Espitalie, J., 1997. Thermal cracking of kerogen in open and closed systems: Determination of kinetic parameters and stoichiometric coefficients for oil and gas generation. Organic Geochemistry 26, 321-339.

Berndt, C., Feseker, T., Treude, T., Krastel, S., Liebetrau, V., Niemann, H., Bertics, V.J., Dumke, I., Duennbier, K., Ferre, B., Graves, C., Gross, F., Hissmann, K., Huehnerbach, V., Krause, S., Lieser, K., Schauer, J., Steinle, L., 2014. Temporal Constraints on Hydrate-Controlled Methane Seepage off Svalbard. Science 343, 284-287.

Bohrmann, G. et al., 2017. R/V MARIA S. MERIAN Cruise Report MSM57, Gas Hydrate Dynamics at the Continental Margin of Svalbard, Reykjavik - Longyearbyen - Reykjavik, 29 July - 07 September 2016. Berichte, MARUM - Zentrum fuer Marine Umweltwissenschaften. Fachbereich Geowissenschaften, Universitaet Bremen, No. 314, 204 pages. Bremen, 2017. ISSN 2195-9633.

Boulter, M.C., Manum, S.B., 1996. Oligocene and Miocene vegetation in high latitudes of the North Atlantic: Palynological evidence from the Hovgård Ridge in the Greenland Sea (Site 908). In Thiede J., Myhre, A.M., Firth, J.V., Johnson G.L., Ruddiman, W.F. (eds.) Proceedings of the Ocean Drilling Program, College Station (TX), (Ocean Drilling Program), Scientific Results, Vol. 151, p. 255-287

Burnham, A.K., Sweeney, J.J., 1989a. A chemical kinetic model of vitrinite maturation and reflectance. Geochimica et Cosmochimica Acta 53, 2649-2657.

Burnham, A.K., Sweeney, J.J., 1989b. Evaluation of a Simple Model of Vitrinite Reflectance Based on Chemical Kinetics. AAPG Bulletin 74, 1559-1570.

Butt, F.A., Elverhoi, A., Solheim, A., Forsberg, C.F., 2000. Deciphering late Cenozoic development of the western Svalbard margin from ODP site 986 results. Marine Geology 169, 373-390.

Bünz, S., Polyanov, S., Vadakkepuliyambatta, S., Consolaro, C., Mienert, J., 2012. Active gas venting through hydrate-bearing sediments on the Vestnesa Ridge, offshore W-Svalbard. Marine Geology 332, 189-197.

Crane, K., Sundvor, E., Buck, R., Martinez, F., 1991. Rifting in the northern Norwegian-Greenland Sea: Thermal tests of assymetric spreading Journal of Geophysical Research 96, 14529-14550.

Dumke, I., Burwicz, E.B., Berndt, C., Klaeschen, D., Feseker, T., Geissler, W.H., Sarkar, S., 2016. Gas hydrate distributionand hydrocarbon maturation north of the Knipovich Ridge, western Svalbard margin. Journal of Geophysical Research: Solid Earth 121, 1405-1424.

Dypvik, H., Riber, L., Burca, F., Ruther, D., Jargvoll, D., Nagy, J., Jochmann, M., 2011. The Paleocene-Eocene thermal maximum (PETM) in Svalbard - clay mineral and geochemical signals. Palaeogeography Palaeoclimatology Palaeoecology 302, 156-169.

Eiken, O., Hinz, K., 1993. Contourites in the Fram Strait. Sedimentary Geology 82, 15-32.

Engen, O., Faleide, J.I., Dyreng, T.K., 2008. Opening of the Fram Strait gateway: A review of plate tectonic constraints. Tectonophysics 450, 51-69.

Faleide, J.I., Solheim, A., Fiedler, A., Hjelstuen, B.O., Andersen, E.S., Vanneste, K., 1996. Late Cenozoic evolution of the western Barents Sea-Svalbard continental margin. Global and Planetary Change 12, 53-74.

Fisher, R.E., Sriskantharajah, S., Lowry, D., Lanoiselle, M., Fowler, C.M.R., James, R.H., Hermansen, O., Myhre, C.L., Stohl, A., Greinert, J., Nisbet-Jones, P.B.R., Mienert, J.,

Nisbet, E.G., 2011. Arctic methane sources: Isotopic evidence for atmospheric inputs. Geophysical Research Letters 38.

Hjelstuen, B.O., Elverhoi, A., Faleide, J.I., 1996. Cenozoic erosion and sediment yield in the drainage area of the Storfjorden Fan. Global and Planetary Change 12, 95-117.

Hustoft, S., Bunz, S., Mienert, J., Chand, S., 2009. Gas hydrate reservoir and active methane-venting province in sediments on < 20 Ma young oceanic crust in the Fram Strait, offshore NW-Svalbard. Earth and Planetary Science Letters 284, 12-24.

Jakobsson, M., Backman, J., Rudels, B., Nycander, J., Frank, M., Mayer, L., Jokat, W., Sangiorgi, F., O'Regan, M., Brinkhuis, H., King, J., Moran, K., 2007. The early Miocene onset of a ventilated circulation regime in the Arctic Ocean. Nature 447, 986-990.

Jakobsson, M., Mayer, L., Coakley, B., Dowdeswell, J.A., Forbes, S., Fridman, B., Hodnesdal, H., Noormets, R., Pedersen, R., Rebesco, M., Schenke, H.W., Zarayskaya, Y., Accettella, D., Armstrong, A., Anderson, R.M., Bienhoff, P., Camerlenghi, A., Church, I., Edwards, M., Gardner, J.V., Hall, J.K., Hell, B., Hestvik, O., Kristoffersen, Y., Marcussen, C., Mohammad, R., Mosher, D., Nghiem, S.V., Pedrosa, M.T., Travaglini, P.G., Weatherall, P., 2012. The International Bathymetric Chart of the Arctic Ocean (IBCAO) Version 3.0. Geophysical Research Letters 39.

Johnson, J.E., Mienert, J., Plaza-Faverola, A., Vadakkepuliyambatta, S., Knies, J., Bunz, S., Andreassen, K., Ferre, B., 2015. Abiotic methane from ultraslow-spreading ridges can charge Arctic gas hydrates. Geology 43, 371-374.

Knies, J., Damm, E., Gutt, J., Mann, U., Pinturier, L., 2004. Near-surface hydrocarbon anomalies in shelf sediments off Spitsbergen: Evidences for past seepages. Geochemistry Geophysics Geosystems 5.

Knies, J., Gaina, C., 2008. Middle miocene ice sheet expansion in the Arctic: Views from the Barents Sea. Geochemistry Geophysics Geosystems 9.

Knies, J., Mann, U., 2002. Depositional environment and source rock potential of Miocene strata from the central Fram Strait: introduction of a new computing tool for simulating organic facies variations. Marine and Petroleum Geology 19, 811-828.

Knies, J., Matthiessen, J., Vogt, C., Laberg, J.S., Hjelstuen, B.O., Smelror, M., Larsen, E., Andreassen, K., Eidvin, T., Vorren, T.O., 2009. The Plio-Pleistocene glaciation of the Barents Sea-Svalbard region: a new model based on revised chronostratigraphy. Quaternary Science Reviews 28, 812-829.

Knies, J., Mattingsdal, R., Fabian, K., Grosfjeld, K., Baranwal, S., Husum, K., De Schepper, S., Vogt, C., Andersen, N., Matthiessen, J., Andreassen, K., Jokat, W., Nam, S.I., Gaina, C., 2014. Effect of early Pliocene uplift on late Pliocene cooling in the Arctic-Atlantic gateway. Earth and Planetary Science Letters 387, 132-144.

Liu, X.L., Flemings, P.B., 2007. Dynamic multiphase flow model of hydrate formation in marine sediments. Journal of Geophysical Research-Solid Earth 112.

Loulergue, L., Schilt, A., Spahni, R., Masson-Delmotte, V., Blunier, T., Lemieux, B., Barnola, J.-M., Raynaud, D., Stocker, T.F., Chappellaz, J., 2008. Orbital and millennial-scale features of atmospheric CH4 over the past 800,000 years. Nature 453, 383-386.

Mann, U., Knies, J., Chand, S., Jokat, W., Stein, R., Zweigel, J., 2009. Evaluation and modelling of Tertiary source rocks in the central Arctic Ocean. Marine and Petroleum Geology 26, 1624-1639.

Matthiessen, J., Brinkhuis, H., Poulsen, N., Smelror, M., 2009. Decahedrella martinheadii Manum 1997-a stratigraphically and paleoenvironmentally useful Miocene acritarch of the high northern latitudes. Micropaleontology 55, 171-186.

Mattingsdal, R., Knies, J., Andreassen, K., Fabian, K., Husum, K., Grosfjeld, K., De Schepper, S., 2014. A new 6 Myr stratigraphic framework for the Atlantic-Arctic Gateway. Quaternary Science Reviews 92, 170-178.

Mau, S., Romer, M., Torres, M.E., Bussmann, I., Pape, T., Damm, E., Geprags, P., Wintersteller, P., Hsu, C.W., Loher, M., Bohrmann, G., 2017. Widespread methane seepage along the continental margin off Svalbard - from Bjornoya to Kongsfjorden. Scientific Reports 7.

Myhre, A.M., Thiede, J., Firth, J.V., al., e., 1995. Proceedings ODP, Initial Reports, 151. Ocean Drilling Program, College Station, TX.

Palumbo, F., Main, I.G., Zito, G., 1999. The thermal evolution of sedimentary basins and its effect on the maturation of hydrocarbons. Geophysical Journal International 139, 248-260.

Panieri, G., Bunz, S., Fornari, D.J., Escartin, J., Serov, P., Jansson, P., Torres, M.E., Johnson, J.E., Hong, W.L., Sauer, S., Garcia, R., Gracias, N., 2017. An integrated view of the methane system in the pockmarks at Vestnesa Ridge, 79 degrees N. Marine Geology 390, 282-300.

Panieri, G., Graves, C.A., James, R.H., 2016. Paleo-methane emissions recorded in foraminifera near the landward limit of the gas hydrate stability zone offshore western Svalbard. Geochemistry Geophysics Geosystems 17, 521-537.

Plaza-Faverola, A., Buenz, S., Johnson, J.E., Chand, S., Knies, J., Mienert, J., Franek, P., 2015. Role of tectonic stress in seepage evolution along the gas hydrate-charged Vestnesa Ridge, Fram Strait. Geophysical Research Letters 42, 733-742.

Plaza-Faverola, A., Vadakkepuliyambatta, S., Hong, W.L., Mienert, J., Bunz, S., Chand, S., Greinert, J., 2017. Bottom-simulating reflector dynamics at Arctic thermogenic gas

provinces: An example from Vestnesa Ridge, offshore west Svalbard. Journal of Geophysical Research-Solid Earth 122, 4089-4105.

Portnov, A., Vadakkepuliyambatta, S., Mienert, J., Hubbard, A., 2016. Ice-sheet-driven methane storage and release in the Arctic. Nature Communications 7.

Poulsen, N.E., Manum, S.B., Williams, G.L., Ellegaard, M., 1996. Tertiary dinoflagellate biostratigraphy of Site 907, 908, and 909 in the Norwegian-Greenland Sea. In Thiede J., Myhre, A.M., Firth, J.V., Johnson G.L., Ruddiman, W.F. (eds.) Proceedings of the Ocean Drilling Program, College Station (TX), (Ocean Drilling Program), Scientific Results, Vol. 151, p. 255-287

Rajan, A., Mienert, J., Bunz, S., Chand, S., 2012. Potential serpentinization, degassing, and gas hydrate formation at a young (< 20 Ma) sedimented ocean crust of the Arctic Ocean ridge system. Journal of Geophysical Research-Solid Earth 117.

Riber, L., 2009. Paleogene depositional conditions and climatic changes of the Frysjaodden Formation in central Spitsbergen (sedimentology and mineralogy, University of Oslo, p. 112.

Ruppel, C.D., 2011. Methane hydrates and contemporary climate change. Nature Education Knowledge 3, 29.

Ryseth, A., Augustson, J.H., Charnock, M., Haugerud, O., Knutsen, S.M., Midboe, P.S., Opsal, J.G., Sundsbo, G., 2003. Cenozoic stratigraphy and evolution of the Sorvestsnaget Basin, southwestern Barents Sea. Norwegian Journal of Geology 83, 107-130.

Sahling, H., Roemer, M., Pape, T., Berges, B., Fereirra, C.d.S., Boelmann, J., Gepraegs, P., Tomczyk, M., Nowald, N., Dimmler, W., Schroedter, L., Glockzin, M., Bohrmann, G., 2014. Gas emissions at the continental margin west of Svalbard: mapping, sampling, and quantification. Biogeosciences 11, 6029-6046.

Sassen, R., Sweet, S.T., Milkov, A.V., DeFreitas, D.A., Kennicutt, M.C., 2001. Thermogenic vent gas and gas hydrate in the Gulf of Mexico slope: Is gas hydrate decomposition significant? Geology 29, 107-110.

Sclater, J.G., Christie, P.A.F., 1980. Continental stretching: an explanation of the post Mid-Cretaceous subsidence of the central North Sea basin. Journal of Geophysical Research 85, 3711-3739.

Shakhova, N., Semiletov, I., Leifer, I., Sergienko, V., Salyuk, A., Kosmach, D., Chernykh, D., Stubbs, C., Nicolsky, D., Tumskoy, V., Gustafsson, O., 2014. Ebullition and storm-induced methane release from the East Siberian Arctic Shelf. Nature Geoscience 7, 64-70.

Smith, A.J., Mienert, J., Bunz, S., Greinert, J., 2014. Thermogenic methane injection via bubble transport into the upper Arctic Ocean from the hydrate-charged Vestnesa Ridge, Svalbard. Geochemistry Geophysics Geosystems 15, 1945-1959.

Stein, R., Boucsein, B., Meyer, H., 2006. Anoxia and high primary production in the Paleogene central Arctic Ocean: First detailed records from Lomonosov Ridge. Geophysical Research Letters 33.

Stein, R., Brass, G., Graham, D., Pimmel, A., 1995. Hydrocarbon measurements at Arctic Gateways Sites (ODP Leg 151), in: Myhre, A.M., Thiede, J., Firth, J.V., Party, L.S.S. (Eds.), Proceedings on ODP, Initial Reports. Ocean Drilling Program, College Station, Texas, USA, pp. 385-395.

Steinle, L., Graves, C.A., Treude, T., Ferre, B., Biastoch, A., Bussmann, I., Berndt, C., Krastel, S., James, R.H., Behrens, E., Boening, C.W., Greinert, J., Sapart, C.-J., Scheinert, M., Sommer, S., Lehmann, M.F., Niemann, H., 2015. Water column methanotrophy controlled by a rapid oceanographic switch. Nature Geoscience 8, 378-382.

Sylta, Ø., 2005. Hydrocarbon migration modelling and exploration risk. Norwegian University of Science and Technology University p. 145.

Sztybor, K., Rasmussen, T.L., 2017. Late glacial and deglacial palaeoceanographic changes at Vestnesa Ridge, Fram Strait: Methane seep versus non-seep environments. Palaeogeography Palaeoclimatology Palaeoecology 476, 77-89.

Vanneste, M., Guidard, S., Mienert, J., 2005. Bottom-simulating reflections and geothermal gradients across the western Svalbard margin. Terra Nova 17, 510-516.

Vogt, P.R., Crane, K., Sundvor, E., Max, M.D., Pfirman, S.L., 1994. Methane-generated(?) pockmarks on young, thickly sedimented oceanic-crust in the Arctic - Vestnesa Ridge, Fram Strait. Geology 22, 255-258.

Westbrook, G.K., Thatcher, K.E., Rohling, E.J., Piotrowski, A.M., Paelike, H., Osborne, A.H., Nisbet, E.G., Minshull, T.A., Lanoiselle, M., James, R.H., Huehnerbach, V., Green, D., Fisher, R.E., Crocker, A.J., Chabert, A., Bolton, C., Beszczynska-Moeller, A., Berndt, C., Aquilina, A., 2009. Escape of methane gas from the seabed along the West Spitsbergen continental margin. Geophysical Research Letters 36.

Whiteman, G., Hope, C., Wadhams, P., 2013. Vast costs of Arctic change. Nature 499, 401-403.

Winkler, A., Wolf-Welling, T.C.W., Stattegger, K., Thiede, J., 2002. Clay mineral sedimentation in high northern latitude deep-sea basins since the Middle Miocene (ODP Leg 151, NAAG). International Journal of Earth Sciences 91, 133-148.

Wolf-Welling, T.C.W., Cremer, M., O`Connell, S., Winkler, A., Thiede, J., 1996. Cenozoic Arctic Gateway paleoclimate variability: indications from changes in coarse-fraction composition, in: Thiede, J., Myhre, A.M., Firth, J.V., Johnson, G.L., Ruddiman, W.F. (Eds.), Proc. ODP, Sci. Results, College Station, TX (Ocean Drilling Program), pp. 515-569.

ACCEPTED MANUSCRIPT

ACCEPTED MANUSCRIPT

ACCEPTED MANUSCRIPT

Knies et al.: Modelling persistent methane seepage offshore western Svalbard since Early Pleistocene

Highlights:

- The modelling results of this manuscript confirms that one of the most dynamic methane hydrate systems in the Arctic was active during the past 2 million years, which is orders of magnitude older than presently known. Hydrocarbons from a Middle Miocene source rock interval have been generated continuously over the past ca. 6 million years.
- Independent from warm and cold climate cycles, the hydrate system off western Svalbard has been continuously fuelled by deeply buried biotic carbon implying that eventually recently reported instabilities of gas hydrate stability zones in this area due to global warming are superimposed effects on long-term natural leakages.

ACCEPTED MANUSCRIPT